Asociación Argentina
de Mecánica Computacional

Mecánica Computacional Vol XLII, pp. 739-748
A. Caggiano, G. Etse, P. Folino, M. Goldschmit, M. Pucheta, M. Storti (Eds.)
S. Giusti, J. Mroginski, P. Sánchez (Issue eds.)
Buenos Aires, November 11-14, 2025

DATA-DRIVEN BAYESIAN DECONVOLUTION OF CONTINUOUS DISTRIBUTIONS OF RELAXATION TIMES

Ligia Ciocci Brazzano[a,b], Leonardo J. Pellizza[b,c], Claudia L. Matteo[a,b], Patricio A. Sorichetti[a], Martín G. González[a,b], Julián Corach[a,b] and Eduardo O. Acosta[a]

[a]*Universidad de Buenos Aires, Facultad de Ingeniería, Dpto. de Física, Grupo de Láser, Óptica de Materiales y Aplicaciones Electromagnéticas, CABA, Argentina*

[b]*Consejo Nacional de Investigaciones Científicas y Técnicas (CONICET), Argentina*

[c]*Institute for Astronomy & Space Physics (UBA/CONICET), CABA, Argentina*

Keywords: Bayesian deconvolution, Data-driven, Mechanical relaxation spectrum, Linear viscoelasticity, Small amplitude oscillatory shear, Uncertainties

Abstract. The knowledge of mechanical properties of materials is based on a precise analysis of their relaxation spectra. The development of methods to deconvolve spectra from measured data, and the assessment of their reliability, is therefore of paramount importance. We present a novel Bayesian deconvolution method based on a physically grounded parameterization of the spectra. We use a Metropolis-Hastings Markov-chain Monte Carlo fitting algorithm, with a full posterior analysis to obtain the best-fitting spectrum and its uncertainties. We test its performance on simulated data, finding that it is unbiased, reliable, and gives precise results even under strong noise.

ISSN: 2591-3522 DOI: 10.70567/mc.v42.ocsid8313

1 INTRODUCTION

An accurate characterization of mechanical properties of solids and liquids is crucial for pure research and technological applications. In the linear viscoelastic regime probed by small-amplitude oscillatory shear (SAOS) techniques, these properties can be modelled assuming that the behaviour of materials is well described by a set of relaxation processes (RPs), known as its relaxation spectrum (RS). Each RP is completely defined by its characteristic timescale and strength, which reveal information about the molecular architecture of the substance (Stadler, 2013). RSa of viscoelastic materials often show a continuous distribution of RPs, represented by a viscosity density H in relaxation time τ (Martinetti et al., 2018). It is usually inferred from measurements of material functions such as the storage G' and loss G'' moduli as a function of the SAOS strain frequency ω (Winter, 1997). These are related to H through a convolution,

$$G^*(\omega) = G_{\text{eq}} + \int_0^\infty H(\tau) K^*(\omega, \tau) \frac{d\tau}{\tau}, \tag{1}$$

where $G^* = G' + \mathbf{i}G''$ is the complex modulus, K^* is a kernel function describing the contribution of an individual RP to G^*, $\mathbf{i}$ is the imaginary unit, and the equilibrium modulus G_{eq} is a positive real constant for viscoelastic solids (null for liquids).

Different techniques have been devised to deconvolve H from measured data of G^*; the assessment of their reliability and their general improvement are therefore key issues to address. The frequently used "discretization method" (DM, e.g. McDougall et al., 2014, and references therein) samples H at a set of N_{DM} abscissas $\{\tau_i\}$, to replace Eq. 1 with

$$G^*(\omega) \approx G_{\text{eq}} + \sum_{i=1}^{N_{\text{DM}}} g_i K^*(\omega, \tau_i). \tag{2}$$

where $g_i = H(\tau_i) \ln(\tau_{i+1}/\tau_i)$. This reduces the problem to a linear regression with free parameters G_{eq} and $\{g_i\}$. This problem is ill-posed, mainly because the convolution in Eq. 1 acts as a low-pass filter dampening rapid variations in H. Conversely, its inversion amplifies the uncertainties present in experimental data, leading to strong high-frequency noise in the deconvolved RS. The DM worsens the problem because the accuracy of the approximation in Eq. 2 increases with N_{DM}. An accurate model requires therefore the introduction of high-frequency components in H, whose dampening leads to parameter degeneracies. Indeed, there is a maximum $N_{\text{DM}} \sim 1.5-2$ RPs per decade above which the fit cannot be further improved, called *parsimonious spectrum* (e.g. Winter, 1997). Note that this small value does not a priori guarantee that the right-hand side of Eq. 2 is a precise estimate of its left-hand side.

To overcome these problems, a lot of effort has been devoted to develop regularization methods that impose mathematical constraints to the fit to keep the solution smooth enough. These methods succeed in reproducing simulated spectra, and give reasonable fits to experimental data, but they provide only an empirical description of the data with little physical insight. An important step forward has been taken by Freund and Ewoldt (2015), who use physically grounded parametric models to describe material moduli, and apply Bayesian techniques to determine the best-fitting parameter set (see Ciocci Brazzano et al., 2016, for a similar technique regarding electrical spectra).

Our aim is to build upon the work of Freund and Ewoldt (2015) by devising a Bayesian method to deconvolve *continuous* spectra, overcoming the limitations of the DM without the need to resort to regularization techniques. Sects. 2 and 3 describe our method and results, respectively, whereas Sect. 4 presents our conclusions.

2 THE METHOD

2.1 Model RS and material moduli prediction

Our method assumes that the *continuous* RS can be modelled by a physically-motivated function $H(\tau;\vec{\theta})$ depending on a small set of parameters $\vec{\theta}$. We adopt as an example a sum of log-normal density functions for $H(\tau)/\tau$,

$$H(\tau) = \sum_{i=1}^{N} \frac{A_i}{\sqrt{2\pi}\sigma_i} \exp\left[-\frac{1}{2}\left(\frac{\ln\tau - \ln\tau_{0,i}}{\sigma_i}\right)^2\right], \tag{3}$$

where the parameters $\vec{\theta} = \{\tau_{0,i}, \sigma_i, A_i\}$ are the mean relaxation time, width, and strength of each RP, respectively. This RS represents a distribution with equal probability for all relaxation states (Tschoegl, 1989). For the kernel describing individual RPs we adopt Maxwell modes,

$$K^*(\omega,\tau) = \frac{(\omega\tau)^2 + \mathbf{i}\omega\tau}{1+(\omega\tau)^2}. \tag{4}$$

We stress that our method is not limited to these choices.

The model prediction for G^* at any frequency ω can be computed to an arbitrary precision level using any algorithm that performs the numerical integration of the right-hand side of Eq. 1. We adopt the standard trapezoidal rule,

$$G^*(\omega|\vec{\theta}) \approx \Delta\lambda \sum_{j=1}^{N_S} a_j H(\tau_j^S|\vec{\theta}) K^*(\omega,\tau_j^S), \tag{5}$$

where all $a_j = 1$ except $a_1 = a_{N_S} = 1/2$, and we use a large number N_S of sampling points τ_j^S defined in an interval $[\tau_{min}, \tau_{max}]$ where the RS has significant values. These points are taken evenly spaced by $\Delta\lambda$ in $\ln\tau$ for simplicity.

It may be argued that this is almost the same approximation of the DM. The subtle but crucial difference is that sampling parameters in Eq. 5 ($N_S, \{\tau_j^S, H(\tau_j^S|\vec{\theta})\}$) are auxiliary numerical quantities, and not fitting parameters like their counterparts in Eq. 2 ($N_{DM}, \{\tau_j, g_j\}$). Decoupling sampling from data fitting allows the former to be dense enough to accurately approximate the integral in Eq. 1, while avoiding overfitting problems (parameter degeneracies, high-frequency fluctuations). Indeed, N_{DM} is limited to 1.5–2 RPs per decade, whereas N_S may be as large as computational power allows. We adopt $N_S \gtrsim 100$ to ensure that numerical errors in the computation of G^* do not affect the fit.

2.2 Data fitting

To estimate the best-fitting RS parameters for some data set $D = \{\omega_k, G_k^*\}$, we maximize the *posterior* probability density function (PDF) of the parameters given D and any previously available information I, $f_{post}(\vec{\theta}|D,I)$. Using Bayes theorem,

$$f_{post}(\vec{\theta}|D,I) = \frac{\mathscr{L}(D|\vec{\theta},I) f_{pri}(\vec{\theta}|I)}{\int_\Theta \mathscr{L}(D|\vec{\theta},I) f_{pri}(\vec{\theta}|I) d\vec{\theta}}, \tag{6}$$

where the *likelihood* $\mathscr{L}(D|\vec{\theta},I)$ is the PDF of D given $\vec{\theta}$ and I, and $f_{pri}(\vec{\theta}|I)$ is the *prior* PDF of $\vec{\theta}$ given I, representing the degree of belief in $\vec{\theta}$ before measuring D.

Our algorithm computes $\mathscr{L}$ using physical assumptions about the nature of the deviation of measured data G^*_k from the model $G^*(\omega_k)$, $G^*_k - G^*(\omega_k) = \Delta G^*_{\text{exp},k} - \Delta G^*_{\text{mod},k}$, with $\Delta G^*_{\text{exp,mod}}$ the deviation of the measured value and the model prediction from the true (unknown) value of the material modulus, respectively. The first term depends on the measurement technique, and is usually assumed to be normally distributed with null mean and dispersion $\sigma_{\text{exp},k}$ defined by the experimental uncertainty. The dispersion may be different at each frequency ω_k, but can be estimated by calibration procedures. The second term arises from the existence of physical effects that are not modelled, for any reason, but are assumed to be small. The distribution of the sum of these effects can be generally described by a Gaussian with null mean and dispersion $\sigma_{\text{mod},k}$. With these hypotheses,[1] $\ln \mathscr{L}(D|\theta, I) = -\chi^2/2$, where

$$\chi^2 = \sum_{k=1}^{N_\text{D}} \frac{\left(G^*_k - G^*(\omega_k)\right)^2}{\sigma^2_{\text{exp},k} + \sigma^2_{\text{mod},k}} \tag{7}$$

is the usual goodness-of-fit statistic. Note that the method is not restricted to $\Delta G^*_{\text{exp,mod}}$ following these assumptions; any hypotheses that give a distribution for them can be used as far as the likelihood can be computed, either analytically or numerically, as in Douna et al. (2015). We also assume a complete lack of previous knowledge, and therefore select a uniform prior f_pri for all parameters.

We use an Markov-chain Monte Carlo technique with a Metropolis-Hastings (MH, e.g., Gregory, 2005) algorithm to perform the maximization. After a short *burn-in* period required to reach the high-probability region of the parameter space Θ, the Markov chain produced by the MH algorithm is by construction a sample distributed as f_post. To infer the best-fitting set of parameters $\vec{\theta}_\text{bf}$, their uncertainties and correlations, we exploit the information contained in this sample. As a first estimate of $\vec{\theta}_\text{bf}$ we use the maximum a posteriori (MAP), obtained directly from the element in the chain with the higher f_post value. Alternative estimates of $\vec{\theta}_\text{bf}$ are the sets of marginal posterior means (MPM) $\langle\vec{\theta}\rangle$, modes $\vec{\theta}_\text{mode}$, and medians $\vec{\theta}_\text{med}$ of the parameters. Marginalizing a Markov chain is done by simply taking one parameter at a time, disregarding the others. Therefore to obtain the MPM of the j-th parameter[2] $\langle\theta_j\rangle$ we compute its sample mean over the chain. To get $\theta_{\text{mode},j}$ we obtain a histogram of θ_j, smooth it, and find the value of θ_j at which it attains its maximum. Finally, to determine $\theta_{\text{med},j}$ we arrange the chain by θ_j in ascending order, and select the value that leaves half of the chain above it.

To assess the uncertainty of the fit for a parameter θ_j, we compute its sample standard deviation over the chain $\theta_{\text{std},j}$. We also calculate marginal $100\,\alpha\%$ credible regions (CRs) as the intervals $[\theta_j^-, \theta_j^+]$ that leave a fraction $(1-\alpha)/2$ of the chain above and below them. To quantify correlations among two parameters θ_j and θ_k we use the standard Pearson correlation coefficient, and to visualize them we determine two-parameter joint CRs. To this aim we compute a smoothed density of chain points in the plane θ_j-θ_k, using a Gaussian kernel. The density contour line that encloses a fraction α of the points defines the $100\,\alpha\%$ CR.

Finally, we propagate the uncertainty estimates to the deconvolved RS and the best-fitting moduli. We compute $H(\tau)$ and $G^*(\omega)$ for each set of parameters in the Markov chain, and for a large set of values of τ and ω. Using these samples, we determine CRs for $H(\tau)$ and $G^*(\omega)$ in the same way as we computed the corresponding CRs for the spectral parameters.

[1] A full derivation under similar hypotheses is given by Freund and Ewoldt (2015).

[2] Note that θ_j denotes the j-th free parameter of the model, whereas $\vec{\theta}_j$ is the j-th set of parameters in the Markov chain.

3 APPLICATION TO SIMULATED AND REAL DATA

To assess the reliability and limitations of our method, we use it in the first place to deconvolve different simulated RSa. We simulate a measured, noiseless data set by using Eq. 5 to convolve $H(\tau)$ with the RP kernel, and obtain G^*_k at N_D data points with frequencies ω_k logarithmically spaced in $[\omega_\mathrm{min}, \omega_\mathrm{max}]$. We choose the values of ω_min, ω_max, and the number of data points per decade $n = N_\mathrm{D}/\log(\omega_\mathrm{max}\,/\,\omega_\mathrm{min})$ to reproduce different experimental data sets. After that, we add Gaussian noise to our simulated data set, with fixed dispersions $\sigma'^{,''}$ for the storage and loss modulus, respectively. We parameterize noise by its peak signal-to-noise ratio,

$$\Sigma'^{,''} = \frac{\max(G'^{,''})}{\sigma'^{,''}}. \tag{8}$$

Notice that this means that the typical signal-to-noise ratio of the data is lower than this value.

3.1 Simulated spectra

As a simple first test, we deconvolved a well sampled RS with very low noise. Left panel of Fig. 1 displays the simulated RS and material moduli, together with different estimates of the best-fitting $H(\tau)$ and $G^*(\omega)$. One of the characteristics of our method is that it gives uncertainty estimates, not only for the parameters but also for the best-fitting H and G^*, which allows a better assessment of the quality of the fit. The method works very well in this case, rendering an extremely tight fit to the data, and recovering the simulated RS within the 68% CR. However, the relative errors of the fit are comparatively greater for H than for G^*. This shows that the RS can deviate from the best-fitting one without significantly changing the material moduli prediction, which is a direct consequence of the convolution that defines the latter, and the root of the ill-posedness of the problem. We note that all estimates of the best-fitting parameters (namely MAP and marginal posterior mean, median and mode) give a good description of the simulated RS to within errors. The deterioration of the precision of the fit in spectral regions far from the peak is a consequence of the smallness of their contribution to G^*.

To investigate the precision and accuracy with which our method recovers the spectral parameters θ_j, we show the posterior distribution of their values obtained from the Markov chain, together with the different estimates of the best-fitting values θ_{bf_j} (Fig. 2). All distributions are unimodal and nearly symmetric, and the standard deviations s_j almost coincide with the 68% CRs. Once again, all estimates of $\theta_{\mathrm{bf},j}$ are close to each other, their differences being lower than s_j. The precision ($\varepsilon_j = s_j/\theta_{\mathrm{bf},j}$) is in the range $0.5-3.5\%$, which is of the same order of the best signal-to-noise ratio in the data (2.5%). Repeating the same simulation several times, we find that the true (simulated) values of the parameters fall at random within the credible regions according roughly to the confidence levels, suggesting that the method is unbiased and therefore its results are good estimates of the true values of the spectral parameters. Notice that the method recovers τ_0 and A with a very high precision ($\lesssim 1\%$), whereas for G_eq and σ the precision decreases (to $\sim 3-4\%$). This is expected for G_eq, as it defines the lower limit of the storage modulus, where noise dominates data. The behaviour of σ deserves further exploration, as it suggests that the fit is not as sensitive to changes in this parameter as for the rest.

We explore the effects of noise on the results of our method, using simulations with different values of the signal-to-noise ratios. For simplicity, we keep $\Sigma' = \Sigma'' = \Sigma$. Right panel of Fig. 1 shows the results of deconvolution of a very noisy spectrum. The fit to G^* is still tight, and the RS is recovered to within uncertainties, indicating that our method performs very well under high noise conditions. As in the high signal-to-noise case, relative errors are higher for the RS

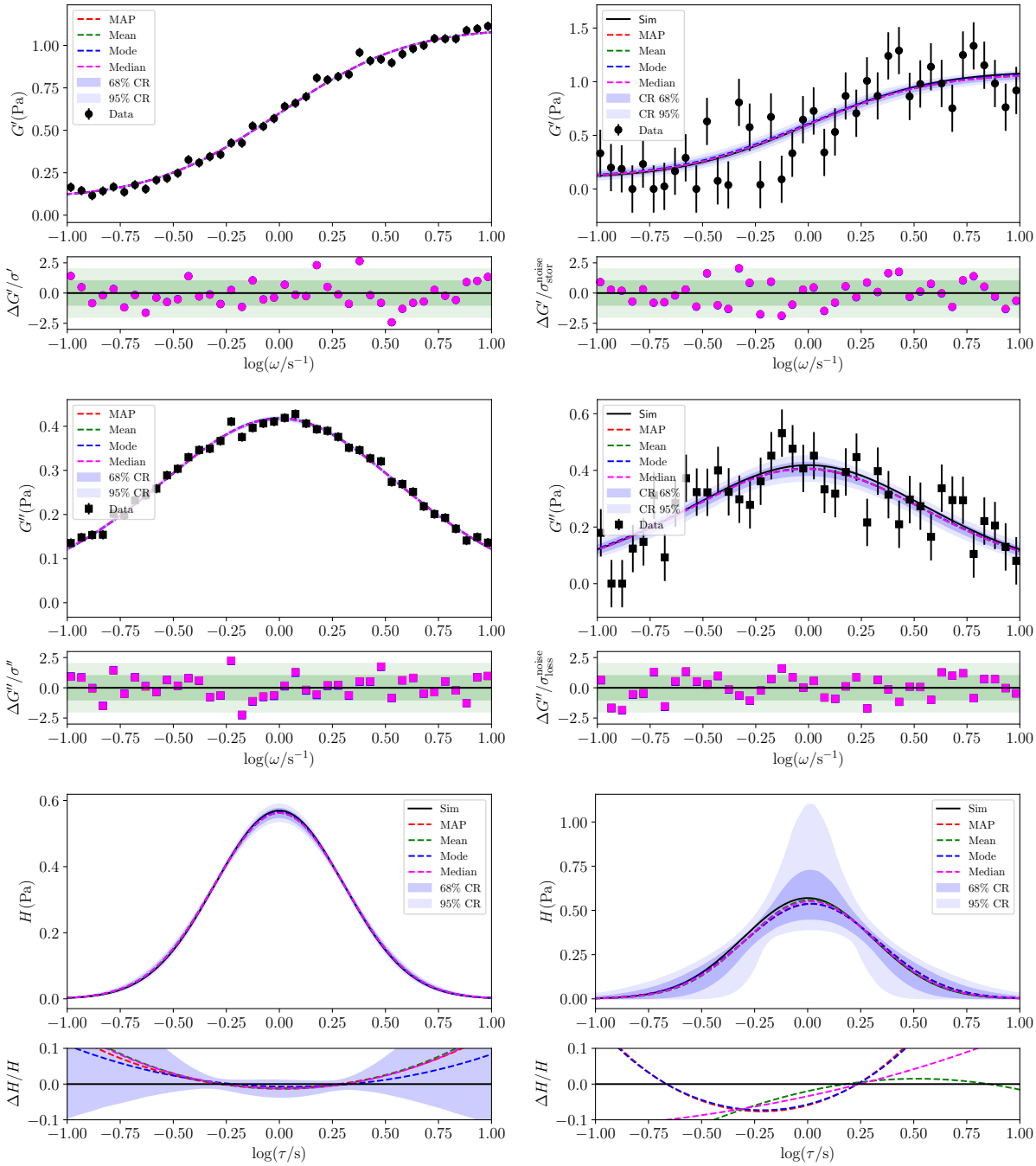

Figure 1: Left panels: Deconvolution of a well sampled, very low noise RS. We show the simulated and best-fitting values (large panels) and goodness-of-fit estimates (small panels) for G' (top), G'' (middle), and H (bottom). The goodness-of-fit for H is estimated by the relative deviation of the fit from the simulated values, whereas for G' and G'' it is represented by the ratio of fit residuals to σ' and σ'', respectively. Green shaded regions mark residuals within $\pm 1\sigma^{\prime,\prime\prime}$ (dark) and $\pm 2\sigma^{\prime,\prime\prime}$ (light). Solid black lines are simulated values, whereas dashed lines are different best-fit estimates: MAP (red), marginal posterior mean (green), mode (blue), and median (magenta). Some lines overlap almost completely due to the smallness of the differences between the estimates. Shaded blue zones are 68% (dark) and 95% (light) CRs. Right panel: Same as left panels, but for a noisy data set ($\Sigma' = \Sigma'' = 5$).

than for the moduli, reflecting the ill-posedness of deconvolution. The only difference with the high signal-to-noise case is that the uncertainties in the best-fitting moduli and spectrum are larger. This is a direct consequence of the larger errors in the data, that make $f_{\rm post}$ shallower

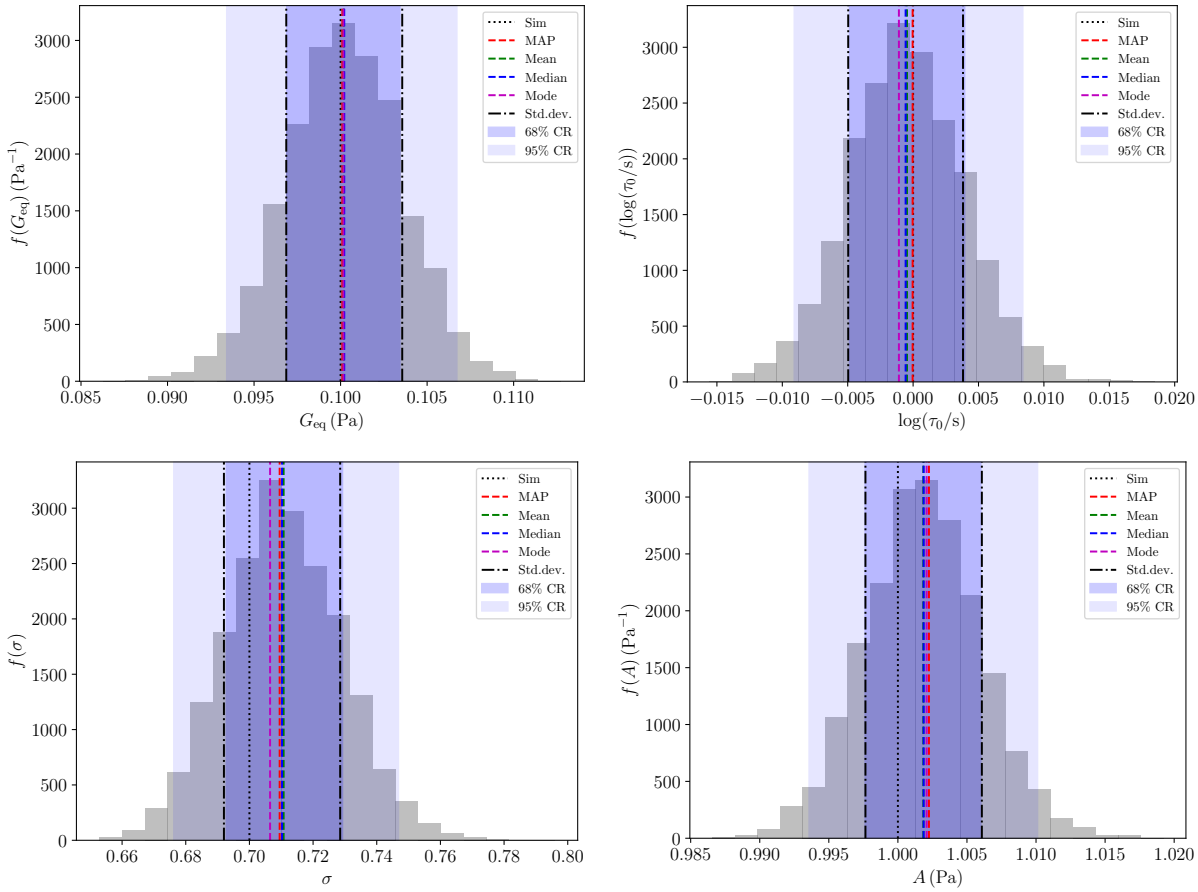

Figure 2: Posterior distribution of parameter values (shaded grey histograms), together with best-fit estimates and uncertainties, for a well sampled, very low noise RS. Dotted black lines are simulated values, whereas dashed lines are different best-fit estimates: MAP (red), marginal posterior mean (green), mode (blue), and median (magenta). Some lines overlap almost completely due to the smallness of the differences between the estimates. Dash-dotted lines indicate ± 1 standard deviations from the median. Shaded blue zones are 68% (dark) and 95% (light) CRs.

and thus enlarge the parameter-space region that provides a good fit. Therefore, the best-fitting spectral parameters are less constrained. Correlations between parameters, on the other hand, are preserved within the signal-to-noise range explored.

3.2 Deconvolution of measured data

Finally, we assess the ability of our method to deconvolve real experimental data. To this aim we use the material moduli data (G' and G'' for 74 frequencies) of the polymer HA12B40 taken from Li et al. (2011). These authors do not present data uncertainties, which gives us also the opportunity to demonstrate that our method is useful even under these conditions. We assume that the relative measurement errors are constant, and adopted a typical value of 4% for them. By visually inspecting the data, we have chosen to try a spectral model with four log-normal components for the fit (13 fitting parameters). These choices show also that our method is versatile enough to use different uncertainty and spectral models (for simulated data we have used constant absolute errors and single-component spectra instead). We performed several fits from random initial guesses and analyzed the distribution of the minimum χ^2 value (Frodesen et al., 1979). The mean value $\langle \chi^2_{\text{min}} \rangle$ obtained was 167. As the expected mean of this statistic (assuming that the spectral and error models are correct) is the number of degrees of freedom

(135 in this case), we deduce that the uncertainties are underestimated by $\sqrt{(167/135)-1} \approx 10\%$, and corrected the relative error estimate to 4.4%. We performed a final fit with this error value, which we show in Fig. 3.

Noise is not especially high in this data set, but we expect edge effects to be present, as storage and loss moduli still grow at the high-frequency end of the data. However, our method manages to obtain an extremely good fit to the data, as it is clearly seen in the upper and middle panels of Fig. 3. Residuals are consistent with a stochastic behaviour of the data around the model for all the estimates of the best-fitting functions. The lower panel shows that also the best-fitting spectrum is very well defined, all estimates differing by less than 10% along the whole relaxation time domain. Fitting uncertainties also remain well under this value except at the large relaxation time end, where they grow beyond this limit. We also show a comparison with the spectrum obtained from the same data by a different method (NLREG, McDougall et al., 2014); the agreement between both methods is fairly good. Small discrepancies are observed near $\log \tau = 0$, where the different estimates made by our method also have the largest disagreement. This could be due to the fact that log-normal components are not the best description for HA12B40 in this relaxation time region, or just an indication that the limit in the description of the spectrum imposed by the ill-posedness of the problem has been reached. Another possibility is that the model requires a fifth component to render a proper description of the spectrum. The fact that the moduli residuals show some evidence of systematic behaviour in the region around $\log \omega = 0$ suggests that the latter is the most probable explanation. It is interesting to note that Bayesian methods such as ours provide a way of treating model comparison problems that is consistent with the Occam razor rule. This would allow our method to assess the model (in this case the number of components) that best describes HA12B40 data. However, the development and testing of such a tool is out of the scope of the present work.

Finally, Fig. 3 shows one of the 78 two-parameter plots describing the covariance of the fitted parameters. As it is clearly seen, the relative uncertainties in these parameters are of the same order of magnitude of the relative experimental errors. This suggests that the method is able to overcome the ill-posedness of the problem and give results limited only by the experimental precision.

4 CONCLUSIONS

We have developed a novel method to deconvolve mechanical RS from storage and loss moduli data as a function of SAOS strain frequency. Our method is based on the concept put forward by Freund and Ewoldt (2015) of using physically motivated, parametric functions to fit material properties. The main difference is that these authors parameterize the storage and loss moduli, whereas we do it with the continuous RS itself. To determine the material moduli that actually fit the data we resort to numerical convolution, computed to an arbitrary precision with standard quadrature methods.

We have tested our method against simulated data representing experimental measurements under different conditions. The method provides a good fit to material moduli regardless of the noise, sampling frequency, or completeness of the data. We have shown that it is unbiased and reliable, in the sense that it recovers always the correct spectral parameters to within fitting uncertainties. Its simplicity and performance make therefore our method an attractive choice for research in material science.[3] Moreover, our method may be improved by adding a Bayesian model comparison module, which would allow to discriminate between models with different

[3]The code is available from the authors upon request.

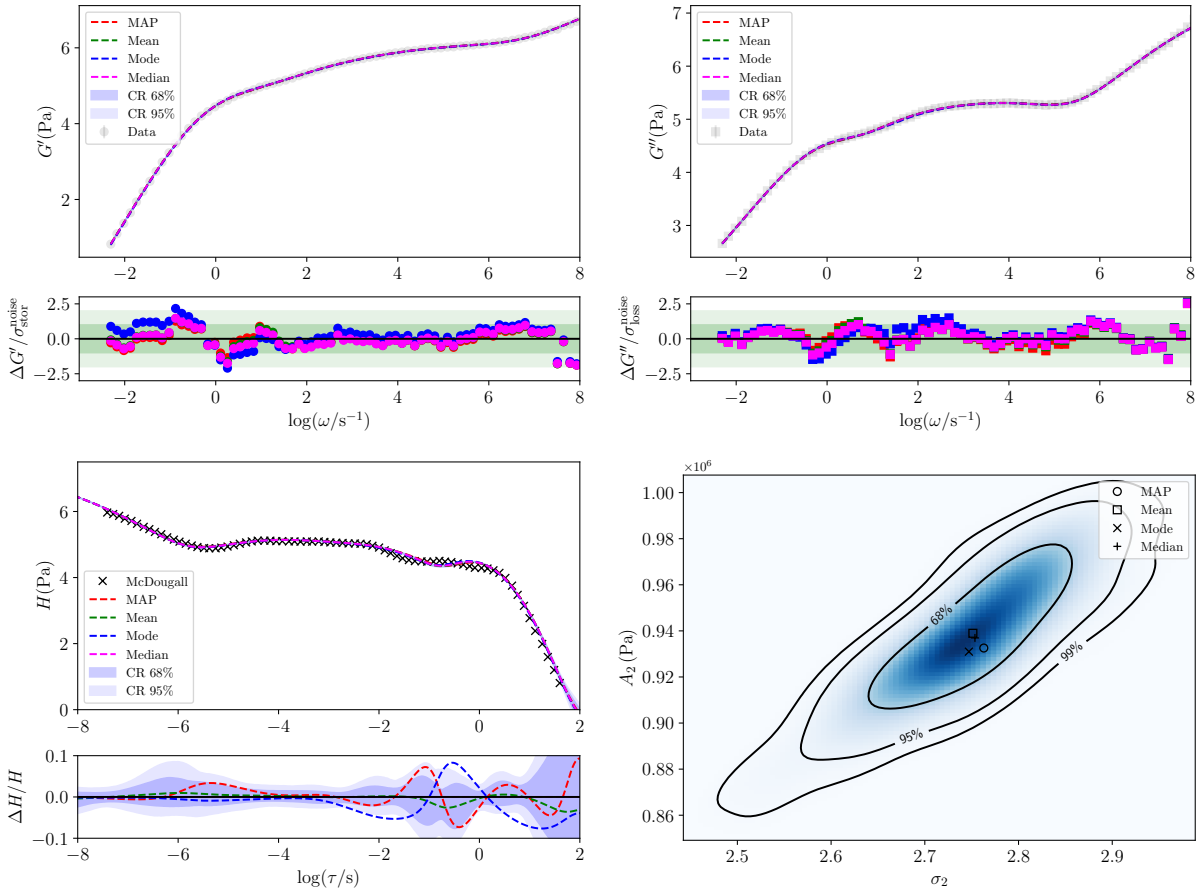

Figure 3: Deconvolution of real data of HA12B40. We show the best-fitting models (large panels) and uncertainty estimates (small panels) for G' (top left), G'' (top right), and H (bottom left). For material moduli we plot also the data (grey circles and squares), whereas for the spectrum we superimpose a fit by McDougall et al. (2014) using the NLREG method, digitized from its Fig. 10 (crosses). The uncertainties for H are estimated by the relative deviation of the fitted spectra from the median estimate, whereas for G' and G'' it is represented by the ratio of fit residuals to σ' and σ'', respectively. Green shaded regions mark residuals within $\pm 1\sigma^{\prime,\prime\prime}$ (dark) and $\pm 2\sigma^{\prime,\prime\prime}$ (light). Shaded blue zones are 68% (dark) and 95% (light) CRs. Right bottom panel: Example of a two-parameter marginal posterior PDF computed from the Markov chain (blue shades) for the fit to experimental HA12B40 data.

number of parameters and thus assess the reality of individual RPs. We are currently developing such a module, and intend to publish it in a follow-up paper.

5 ACKNOWLEDGEMENTS

This work was supported by Universidad de Buenos Aires (UBACyT grants 20020190100275BA, 20020190200255BA, and 20020190100032BA), by ANPCyT (PICT grants 2020-0582, and 2022-03741) and by CONICET (PIP grants 11220200102112CO, and 11220200101826CO).

REFERENCES

Ciocci Brazzano L., Pellizza L.J., Matteo C.L., and Sorichetti P.A. A Bayesian method for analysing relaxation spectra. *Computer Physics Communications*, 198:22–30, 2016. http://doi.org/https://doi.org/10.1016/j.cpc.2015.08.033.

Douna V.M., Pellizza L.J., Mirabel I.F., and Pedrosa S.E. Metallicity dependence of high-mass X-ray binary populations. *Astronomy & Astrophysics*, 579:A44, 2015.

http://doi.org/10.1051/0004-6361/201525617.

Freund J.B. and Ewoldt R.H. Quantitative rheological model selection: Good fits versus credible models using Bayesian inference. *Journal of Rheology*, 59(3):667–701, 2015. http://doi.org/10.1122/1.4915299.

Frodesen A.G., Skjeggestad O., and Tofte H. *Probability and Statistics in Particle Physics*. Universitetsforlaget, Bergen, Norway, 1979.

Gregory P.C. *Bayesian logical data analysis for the physical sciences: a comparative approach with Mathematica support*. Cambridge University Press, 2005. http://doi.org/https://doi.org/10.1017/CBO9780511791277.

Li S.W., Park H.E., and Dealy J.M. Evaluation of molecular linear viscoelastic models for polydisperse h polybutadienes. *Journal of Rheology*, 55(6):1341–1373, 2011.

Martinetti L., Soulages J.M., and Ewoldt R.H. Continuous relaxation spectra for constitutive models in medium-amplitude oscillatory shear. *Journal of Rheology*, 62(5):1271–1298, 2018. http://doi.org/10.1122/1.5025080.

McDougall I., Orbey N., and Dealy J.M. Inferring meaningful relaxation spectra from experimental data. *Journal of Rheology*, 58(3):779–797, 2014. http://doi.org/10.1122/1.4870967.

Stadler F.J. On the usefulness of rheological spectra – a critical discussion. *Rheologica Acta*, 1(52):85–89, 2013.

Tschoegl N.W. *The phenomenological theory of linear viscoelastic behavior*. Springer Verlag, 1989. http://doi.org/10.1007/978-3-642-73602-5.

Winter H. Analysis of dynamic mechanical data: Inversion into a relaxation time spectrum and consistency check. *J. Non-Newtonian Fluid Mech.*, 68(2-3):225–239, 1997. http://doi.org/https://doi.org/10.1016/S0377-0257(96)01512-1.